Chapter

The Role of CFD in Modern Jet Engine Combustor Design

Zhi X. Chen, Ivan Langella and Nedunchezhian Swaminathan

Abstract

Recent advances in the application of computational fluid dynamics (CFD) for turbulent combustion with the relevance for gas turbine jet engines are discussed. Large eddy simulation (LES) has emerged as a powerful approach to handle the highly turbulent, unsteady and thermochemically non-linear flows in the practical combustors, and it is a matter of time for the industry to replace the conventional Reynolds averaged Navier-Stokes (RANS) approach by LES as the main CFD tool for combustor research and development. Since combustion is a subgrid scale phenomenon in LES, appropriate modelling is required to describe the SGS combustion effects on the resolved scales. Among the various available models, the flamelet approach is seen to be a promising candidate for practical application because of its computational efficiency, robustness and accuracy. A revised flamelet formulation, FlaRe, is introduced to outline the general LES methodology for combustion modelling and then used for a range of test cases to demonstrate its capabilities for both laboratory burners and practical engine combustors. The LES results generally compare well with the experimental measurements showing that the important physical processes are captured in the simulations.

Keywords: jet engine combustion, computational fluid dynamics, large eddy simulation, turbulent combustion modelling, FlaRe

1. Introduction

Over the past half a century, the combustor design for jet engines has been driven to meet the increasingly higher standards of thermal efficiency, emission reduction and power-to-size/weight ratio. Consequently, the operating conditions have experienced a dramatic change, e.g., the operating pressure increasing from several bars to few tens of bars, combustor inlet temperature from about 500 to nearly 1000 K, and turbine inlet temperature from just above 1000 to almost 2000 K in today's turbo-fan engines [1]. Despite the severe change in the fluid-mechanical and thermodynamic properties of the combustor internal flow, the combustor length and frontal area are still strictly limited by the design factors for other engine components. Also, the current unprecedented demand for global travels requires a much longer lifespan for aero engines, typically many tens of thousands of hours without major maintenance. To meet these requirements, jet engine manufacturers continuously seek avenues for a reliable, efficient and economical combustor design cycle.

The emergence of computational fluid dynamics (CFD) has made computer-aided design an integral part of the gas turbine (GT) combustor design process [2].

Compared to the expensive experimental tests, which provide only global information (e.g., stability, outlet properties), CFD is much cheaper to run and, most importantly it can be repeated during the design process to examine the effects of small design changes. Thus, it is attractive for practical applications. Over the recent years, there has been a significant increase in the investment from the industry for the development of CFD tools, but the challenges remain because fully resolving the turbulent reacting flows in practical jet engines using direct numerical simulation (DNS) is still far beyond our reach. The Reynolds averaged Navier-Stokes (RANS) approach has been broadly used as the main CFD tool for practical combustor design in the last few decades. Because all the scales are modelled in RANS, only mean flow quantities are computed leading to a cheap and fast calculation. For steady combusting flows, good accuracy can be achieved if the correlation between the fluctuating quantities is handled correctly. The drawback for RANS is also obvious since the transient phenomena, such as ignition, flashback, thermoacoustics and blow-off, cannot be captured by the mean flow calculation. While these phenomena are of high interest for the industry, there is an increasing need for predictive CFD tools. Large eddy simulation (LES) is recognised as a promising candidate as the energy-containing flow structures are directly resolved by the numerical grid and the subgrid scales (SGS) are modelled. In general, with respect to RANS the main advantages of LES are twofold: the capability to capture the transient phenomena and a better prediction of mixing. Thus, the LES modelling paradigm is of interest here.

The level of resolved scales in LES dictates the computational cost, i.e., the more resolved the more expensive; however, it only partly determines the overall accuracy. A significant part of the accuracy is attributed to SGS modelling, which represents the influence of subgrid motion on the resolved scales. For the velocity field, this influence usually appears through the SGS eddy viscosity and in a well-resolved LES, i.e., typically over 80% of the turbulent kinetic energy is resolved [3], the SGS effect is relatively small. For the flame, however, chemical reactions occur at scales smaller than the typical LES filter size and thus are SGS phenomena requiring closure models. The major challenge is how to model the SGS interaction between turbulence and chemistry, with the latter involving a large number of species and reactions (typically many thousands for common jet fuels). Consequently, this makes it practically unfeasible to directly integrate detailed chemical kinetics into the LES. Finding a computationally efficient model with good accuracy and robustness for the SGS turbulence-chemistry interaction has been a central topic for turbulent combustion research in the last two decades, and a number of approaches are available in the literature. Extensive review of these approaches is beyond the scope of this chapter as detailed reviews are available elsewhere, see for example [2–5], and the focus here is to showcase the current capabilities of combustion LES modelling for practical applications.

The rest of this chapter is organised as follows. Section 2 describes the modelling challenges in LES of gas turbine combustion and a representative approach to tackle these challenges. The validation test cases for this approach are presented in Sections 3 and 4 for laboratory and practical burners respectively. The conclusions are summarised with a future outlook in Section 5.

2. State-of-the-art LES modelling for gas turbine combustion

With the advent of high performing computing, large eddy simulation has become increasingly popular to investigate complex and unsteady physics in gas turbines due to its versatility in capturing time-dependent phenomena and in

controlling the computational effort at the same time. This is achieved by varying the LES filter, whose shape is implicit and depends on local mesh size, SGS model and numerical scheme. It is generally accepted that the filter size is proportional to the local cell volume, $\Delta \approx \mathcal{V}^{1/3}$. The larger is Δ, the stronger is the contribution of the SGS modelling to the results, with the generally accepted rule that at least 80% of the turbulent kinetic energy should be resolved [3]. The general LES equation for a quantity φ takes the form, in Einstein's notation,

$$\frac{\partial \overline{\rho}\tilde{\varphi}}{\partial t} + \frac{\partial \overline{\rho}\tilde{u}_i\tilde{\varphi}}{\partial x_i} = -\frac{\partial \overline{\rho}}{\partial x_j} + \overline{\mathcal{D}} + \frac{\partial \overline{\tau}}{\partial x_i} + \overline{S}, \tag{1}$$

where the overbar denotes a spacial filtering operation. For density varying flows the filtering operation would lead to additional unclosed terms and to avoid this a density-weighted, or Favre-filtered operator is introduced, defined as $\tilde{\varphi} = \overline{\rho\varphi}/\overline{\rho}$. Note that as $\overline{\varphi} \neq \tilde{\varphi}$, one has to be mindful when comparing CFD results with measurements in regions of strong density gradients, and this will be discussed again in Section 4. The terms on the LHS of Eq. (1) represent time variation and convection of the filtered quantity $\tilde{\varphi}$. The pressure derivative on the RHS in present only if φ is a velocity component, u_j. The application of the LES filter to the convective term leads to the appearance of the term $\overline{\tau} = \overline{\rho}(\widetilde{u_i\varphi} - \tilde{u}_i\tilde{\varphi})$ representing the effect of subgrid processes, and this term requires modelling. Well accepted models are available, e.g., the Smagorinsky model [6] for SGS stresses and the gradient transport model for unresolved scalar fluxes [2]. The filtered diffusion term, $\overline{\mathcal{D}}$, takes the form of a Laplacian and also may need modelling. However, this modelling is generally irrelevant for most high-turbulent conditions proper of gas turbines since the SGS turbulent diffusion is dominant. The last term in Eq. (1) is the filtered source term representing compressibility, or gravitational, or evaporation or heat release effects. For the equation of species the source term is the reaction rate and its modelling is the objective of this section.

For industrial gas turbine conditions the flame thickness, δ, is generally small, so to keep the computational cost affordable for industrial operations, Δ is always larger than δ and thus the combustion processes are entirely at SGS level. Note that it is not generally a problem to satisfy the 80% rule, since the evaluation of the turbulent kinetic energy excludes the combustion dilatation effects [3, 7]. In light of the above considerations, recent development of combustion modelling has gone in two directions. One is to include the full thermochemistry into the modelling, and at the expenses of computational cost. These types of modelling are usually unaffordable for industrial design purposes, but together with DNS methodology they can be used to investigate complex phenomena and SGS processes in laboratory scale burners. The other approach is more industrial-oriented, where the objective is to keep the computational cost to a minimum so that the model is usable for practical combustors. The thermochemistry is included through statistical or geometrical means. Based on this distinction, these two directions can be categorised respectively as non-flamelet and flamelet approaches. The gap in the accuracy between these two categories has reduced with time and recent advances have shown that flamelet-based models are capable of representing the complex flow features in gas turbines despite the limitations of their underlying assumptions. These models are reviewed in a number of works, see for example [2, 4, 8]. Because of the relevance for gas turbine applications, only the flamelet category is discussed here. Within the flamelet category there are geometrical and statistical approaches. Although in both cases the thermochemistry is computed *a priori*, the assumptions behind geometrical models usually lead to the need of relatively large mesh in order to achieve a significant increase of accuracy, see for example the

discussion on thickened flame [9, 10] model in Section 4, or the introduction of additional complexity to smooth the G-equation in level set models [11–13]. Thus, the use of this category of models for industrial applications is still unclear. The statistical models within the flamelet approach include the turbulence-chemistry interaction using probability density functions (PDFs), which are typically presumed and thus they do not incur additional computational effort. Although additional equations are still necessary depending on the particular model, these are generally computationally cheap to solve because the filter size can be kept larger than the flame thickness, at least in principle, as long as the presumed PDF used is able to represent the statistical behaviour at scales smaller than Δ correctly. The potential of flamelet-based models for GT applications has thus to pass through a deep understanding of the SGS processes, which has been the focus of research in the last 30 years. Only in recent years, however, revised flamelets formulations for LES have demonstrated potentials to bridge the gap that separated them from models directly accounting for the thermochemistry.

In flamelet models, the turbulent flame is seen as an ensemble of thin, one-dimensional structures (flamelets) which are wrinkled by turbulence; turbulent eddies are either not small enough to penetrate into the flame and alter its internal structure, or they do not last long enough. Therefore, the thermochemistry can be computed *a priori* through one-dimensional computations and then parameterised using a set of control variables. For partially premixed combustion these are usually a variable to track the rate of mixing, and another to track the reaction progress. Other parameters can be introduced to include additional effects such as pressure variation, non-adiabaticity, strain, etc. The 1D laminar flames can be of any type, e.g. they can be premixed or diffusion flame. Premixed flamelets are, however, more versatile for partially premixed combustion as strain, reaction progress and mixing can be controlled independently; thus they can, in principle, be used for situations involving local extinctions. The big challenge for using flamelet models for GT combustion conditions is that turbulence is extremely high and the smallest eddies can penetrate and affect the internal flame structure, thus invalidating the flamelet hypothesis. This can happen when the Karlovitz number, $Ka = \tau_c/\tau_\eta \gg 1$, where τ_c and τ_η are chemical and the Kolmogorov time scales respectively. Nevertheless, a number of relatively recent works (see for example [14–16]) have shown that flamelet structures are present at GT combustion conditions, but distributed over a wider region yielding a thicker flame brush rather than a thicker flame.[1] This is because small eddies may not have enough energy to impart significant changes to the flame structures [17, 18] and thus the limits of applicability of premixed flamelets are unclear [2, 19].

For stable GT combustion conditions the pressure across the flame does not vary significantly and thus different flamelets for different pressures are not typically computed. The effect of heat losses is also generally taken to be small for combustion modelling purposes. The effect of strain on a premixed flamelet is well accepted to be important in the case of RANS simulations, however its relevance for LES is more controversial. Recent findings [20, 21] show that, since part of the strain is resolved in the LES, its effect on the flame is implicitly captured as long as the local mesh size is appropriate. These preliminary findings have been confirmed by GT calculations [22–24] and show that strained flamelets are unnecessary at least for the conditions considered. For an industrial perspective where the reduction of computational cost is essential, these recent findings open the way to effective use

[1] The flame brush is the time-averaged high temperature region. Hence, it can be thick despite the flame being thin when the flame moves or is distributed spatially.

of flamelets. Following the above discussion, the parameterisation of a model based on unstrained premixed flamelets at various equivalence ratios reduces to only two controlling variables: mixture fraction, ξ, to track the amount of mixing (thus the equivalence ratio) and a progress variable, c, to track the reaction progress. The first is usually defined using Bilger's expression [25], and assuming that all species have the same mass diffusivity, its transport equation is:

$$\overline{\rho}\frac{D\tilde{\xi}}{Dt} = \nabla \cdot \left(\overline{\rho}\mathcal{D}_{eff}\nabla\tilde{\xi}\right) + \overline{\dot{\omega}}_S, \tag{2}$$

where $\mathcal{D}_{eff}$ is the effective molecular diffusivity (sum of filtered diffusivity and the SGS contribution due to the filtering of the non-linear terms). The source term, $\overline{\dot{\omega}}_S$, is for the evaporation of fuel droplets [23, 26, 27]. The progress variable is usually defined as a combination of reactant or product species and varies monotonically from 0 in the reactants to 1 in the products when it is normalised appropriately, although unscaled formulations are often used. A good choice for lean combustion is to define the progress variable as a linear combination of CO_2 and CO [28] mass fractions (normalised by their burnt value). The transport equation for the filtered progress variable is:

$$\overline{\rho}\frac{D\tilde{c}}{Dt} = \nabla \cdot \left(\overline{\rho}D_{eff}\nabla\tilde{c}\right) + \overline{\dot{\omega}}_c^*, \tag{3}$$

where $\overline{\dot{\omega}}_c^*$ is the modified filtered reaction rate, which is tabulated and thus is accessed using the controlling variables themselves during the simulation runtime. This term is expressed as $\overline{\dot{\omega}}_c^* = \overline{\dot{\omega}}_c + \overline{\dot{\omega}}_{np} + \overline{\dot{\omega}}_{ct}$, where $\overline{\dot{\omega}}_c$ is the premixed flame contribution (including mixture stratification). The additional terms represent non-premixed mode contribution and mixed mode due to the interaction of ξ and c gradients, and they appear only for normalised definitions of the progress variable, see additional details for example in [22, 25, 29]. At this point the set of equations would be closed if the above reaction rates depend only on the two controlling variables, as long as a thermodynamic model is provided. However, in this form the effect of wrinkling of the flame by turbulence at the subgrid level is not accounted. This effect is introduced in a statistical way using a presumed subgrid PDF[2]:

$$\overline{\dot{\omega}}_c = \int_0^1\int_0^1 \dot{\omega}(\zeta,\eta)P(\zeta,\eta)d\zeta d\eta, \tag{4}$$

where $\dot{\omega}$ is the laminar reaction rate from the flamelet and ζ and η are the sample space variables for c and ξ respectively. This type of closure was first introduced by Bradley for RANS and non-premixed combustion [30]. The SGS joint PDF can be written as the product of two PDFs as $P(\zeta,\eta) = P(\zeta)P(\eta|\zeta)$. There are various possible choices for the shape of these two SGS PDFs, each with its own advantages and disadvantages, the most common being the Beta PDF and laminar flamelet PDF [31], and it is commonly accepted that these shapes need to be dependent at least on first and second moments. However, for cases involving large turbulence and filter sizes larger than the flame thickness, the Beta PDF was shown to be more

[2] Note that the term PDF in this case does not strictly relates to a probability density function in a statistical sense, since in the LES this operator is used to account for events in space at one time. The use of the term subgrid PDF is thus made for simplicity and analogy to the statistical PDF operator; other authors prefer the term 'filtered density function' to make this distinction.

appropriate in several works (see for example [20, 32–36]). The beta function requires the first and second moments, thus the SGS joint PDF is expressed as $P(\zeta,\eta) = \beta(\zeta;\tilde{c},\sigma_c^2)\beta\left(\eta|\zeta;\tilde{\xi},\sigma_\xi^2\right)$, where σ_c^2 and σ_ξ^2 are the SGS variances of the progress variable and mixture fraction respectively. Note that here the two PDFs are treated independently, which is usually acceptable in LES with an appropriate grid size [37]. The SGS variances obtained using their transport equations are better than using algebraic expressions since convective and diffusive processes are important at subgrid scales [20]. These equations are written as:

$$\overline{\rho}\frac{D\sigma_\xi^2}{Dt} = \nabla\cdot\left(\mathcal{D}_{eff}\nabla\sigma_\xi^2\right) - 2\overline{\rho}\tilde{\varepsilon}_\xi + 2\overline{\rho}\frac{\nu_t}{Sc_t}\left(\nabla\tilde{\xi}\cdot\nabla\tilde{\xi}\right) + \overline{\rho}S, \tag{5}$$

for the mixture fraction variance, and

$$\overline{\rho}\frac{D\sigma_c^2}{Dt} \approx \nabla\cdot\left(\mathcal{D}_{eff}\nabla\sigma_c^2\right) - 2\overline{\rho}\tilde{\varepsilon}_c + 2\overline{\rho}\frac{\nu_t}{Sc_t}\left(\nabla\tilde{c}\cdot\nabla\tilde{c}\right) + 2\left(\overline{c\dot{\omega}} - \tilde{c}\,\overline{\dot{\omega}}\right) \tag{6}$$

for the SGS variance of progress variable. From left to right the various terms in the above equations represent total derivative, effective diffusion, scalar dissipation, turbulent production and source term. The evaporation of droplets contributes to σ_ξ^2 and the subgrid reaction processes contribute to σ_c^2. The latter is closed with an expression consistent with Eq. (4). The evaporation and the spray model in general are out of the scope of this section. For the specific simulations to be presented in Section 4, a Lagrangian approach is used for the two-phase flow, with parcel sampled using a Rosin-Rammler distribution and the Sattelmayer correlation for the initial Sauter mean diameter (SMD) [38]. Only secondary breakup is considered using the process described in [39], and a rapid mixing formulation for the droplet evaporation. More details can be found in [23, 27, 40].

The scalar dissipation rate (SDR) terms in Eqs. (5) and (6) need closure. The linear relaxation model, $\tilde{\varepsilon}_\xi = C_\xi\left(\nu_t/\Delta^2\right)\sigma_\xi^2$, with $C_\xi \approx 2$, is well accepted [5]. Recent works have suggested that this constant is to be revised in case of liquid fuel due to the evaporation source term in Eq. (5) [27]. For the progress variable SGS variance, it is shown in [20] that the reactive term in this equation is of leading order at least for Δ of sizes comparable or larger than the flame thickness, and thus the SDR has to balance the sources coming from reaction and turbulence. Hence, the linear relaxation model is unsuitable on physical grounds. To justify the use of linear relaxation model, a delta or three-delta function is used sometimes instead of the Beta function in Eq. (4) so that $\left(\overline{c\dot{\omega}} - \tilde{c}\,\overline{\dot{\omega}}\right) = 0$ in Eq. (6). This, however, creates a conflict since the meaning of σ_c^2 changes without the reactive term. More recently, revision of the flamelet modelling in the context of LES to take into account the correct reaction-turbulence-diffusion balance led to appearance of more sophisticated, yet simple, model for the SDR of progress variable. One recent development in this sense is the SDR closure of Dunstan et al. [41], which approaches the linear relaxation concept in the limiting behaviour of non-reactive mixture and is thus more recommended. This model has been used in many past studies for different combustion regimes [20, 22, 24, 36] (see also Sections 3 and 4).

The set of equations shown above is used in conjunction with the LES equations for mass and momentum, which are the same for reacting and non-reacting flows, see for example [2, 3] for a more detailed explanation. In principle, the temperature and density fields can be also computed *a priori* using an equation consistent to (4) and accessed in runtime using the controlling variables. In order to account for possible non-adiabatic

effects, an energy equation is often solved. For low-Mach conditions it is convenient to use a total specific enthalpy (sum of formation and sensible enthalpies), which is a conserved quantity. The equation for the filtered total enthalpy, $\tilde{h}$, has the same form of Eq. (2) (except for thermal diffusivity in place of mass diffusivity and no source term). The temperature field is obtained using $\tilde{h}$ by inverting the following expression:

$$\tilde{h} = \widetilde{\Delta h_f^0} + \int_{T_0}^{T} \tilde{C}_p(T)\ dT \tag{7}$$

where Δh_f^0 is the enthalpy of formation of the mixture at temperature T_0 and C_p is the heat capacity at constant pressure. This inversion can be performed numerically in different ways, see for example [20, 23, 42], and requires the integration of enthalpy of formation and heat capacity using an equation consistent to Eq. (4). The density is computed via the state equation, where the pressure is often assumed to be constant in low-Mach formulations for numerical stability, except for cases where compressibility effects are important, e.g. thermoacoustic instabilities. The above equations describe the general flamelet formulation with specific details for the FlaRe approach. In the next sections specific test cases relevant for gas turbine engines will be discussed using both laboratory and practical flames, and the FlaRe approach is compared to other combustion model results where they are available.

3. Laboratory burners

For practical jet engines, it is technically difficult and very costly to conduct measurements inside the combustion chamber due to the extremely hostile conditions and complex geometry. Therefore, laboratory burners not only play a crucial role in experimental combustion research but also serve as a main source for CFD model validation. In the past, the majority of the modelling efforts were devoted to flames in simple geometry such as jet flames and bluff-body or swirl stabilised flames in an open environment. Many of these flames have been benchmarked as standard model validation cases documented in the well-known TNF Workshop [43]. Over the last few decades, a large number of combustion models including most of those discussed earlier in Section 2 have been tested using the TNF benchmark flames [44]. Despite the different models used, the computational results converge to a similar level of very satisfactory accuracy when compared with measurements for the main flow and flame statistics. For example, the transient ignition of a lifted methane-air jet flame [45] was simulated using FlaRe [46], conditional moment closure (CMC) [47], thickened flame (TF) [48] and transported PDF with Eulerian stochastic fields (TPDF/ESF) [49] approaches, all showing comparably good agreement with the measurements for the flame upstream propagation. However, this level of general agreement among different models is yet to be achieved for more complex engine-relevant geometry and conditions. Therefore, this section focuses on the state-of-the-art laboratory gas turbine model combustors (GTMCs). In order to demonstrate the current CFD capabilities of tackling the various issues in these combustors, two cases, for single and multiple burner configurations, are considered.

3.1 Single burner with dual swirlers

The dual-swirl GTMC experimentally investigated by Meier et al. [50, 51] at the German Aerospace Center (DLR) is of interest. The schematic of this GTMC

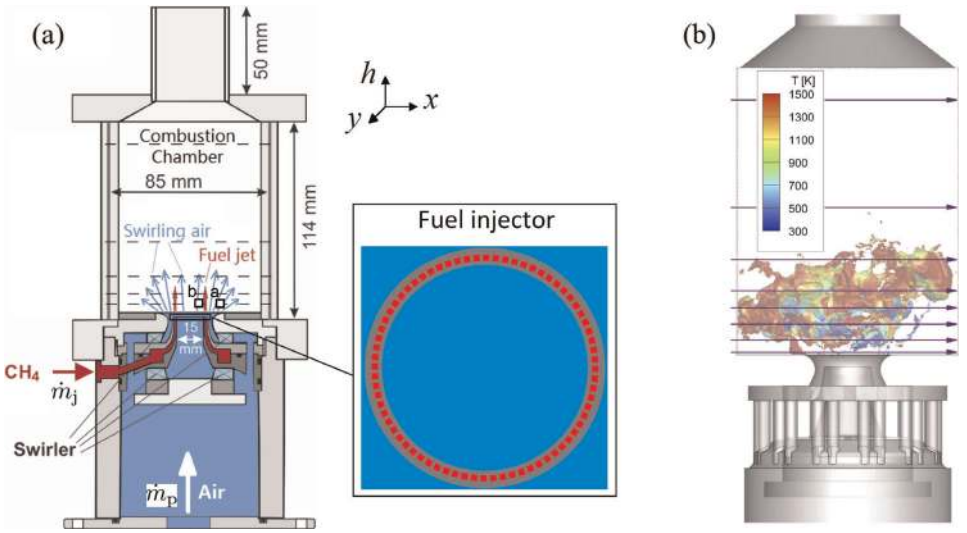

Figure 1.
The DLR dual-swirl combustor: (a) schematic of the experimental setup and (b) typical flame surface marked using $\overline{\dot{\omega}}_c^* = 200$ kg/m³/s, coloured by temperature.

[50, 51] and a typical computed flame surface using LES [24] are shown in **Figure 1**. This burner has a single nozzle head with dual-swirl air passages, which is a common design in modern jet engines to achieve fast fuel-air mixing. The methane gas injector was modified from a practical air-blasting liquid fuel injector mounted on the wall in between the two air nozzles. The experiments were conducted at atmospheric pressure and the operating range investigated was from 5 to 35 kW with the equivalence ratio varying from 0.5 to 1.2, which are typical jet-engine relevant conditions [1].

Within the range of conditions operated, a variety of phenomena were observed including flame-vortex interaction [52], self-excited thermo-acoustic oscillations [53] and lean blow-out (LBO) dynamics [54] in the experiments. Three cases detailed in **Table 1** were chosen for experimental study: a thermo-acoustically stable flame, designated as flame A, an unstable flame showing self-excited thermoacoustic oscillations, called flame B, and flame C exhibiting periodic blowout and re-ignition. To investigate the rich physics exhibited in these flames, state-of-the-art laser diagnostic techniques including stereoscopic particle image velocimetry (stereo-PIV), Raman spectroscopy, laser Doppler velocimetry (LDV), OH^*/CH^* chemiluminescence and $OH/CH/CH_2O$ planar laser-induced fluorescence (PLIF), were performed and highly repetitive results were obtained. Hence, these measurements constitute a comprehensive database for rigorous combustion model assessment.

As noted earlier, only typical results are presented here for a brief demonstration of the model performance. **Figure 2** compares the measured and computed mean

Flame	ϕ_{glob}	Z_{glob}	$\dot{m}_p$ [g/s]	$\dot{m}_j$ [g/s]	Swirl number	P_{th} [kW]
A (stable)	0.65	0.037	18.25	0.697	0.9	34.9
B (unstable)	0.75	0.042	4.68	0.205	0.55	10.3
C (approaching LBO)	0.55	0.031	4.68	0.15	0.55	7.6

Table 1.
Summary of operating conditions.

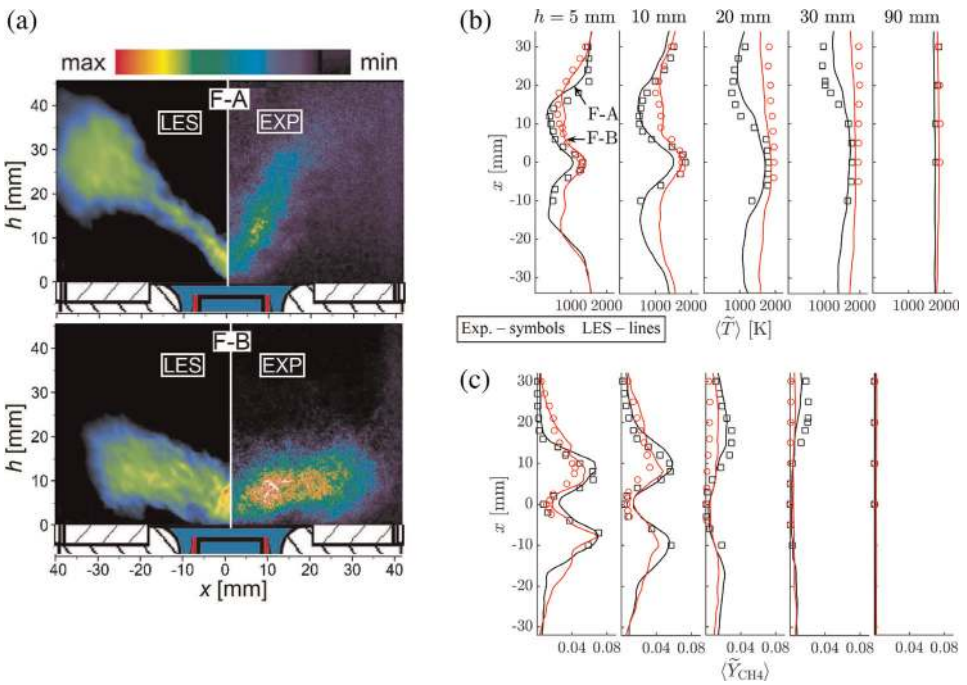

Figure 2.
Typical comparison between LES results and measurements for flames A and B: (a) mid-plane mean concentration of CH radials, mean radial variation of (b) temperature and (c) fuel mass fraction.

reaction zone shape (represented by CH radials), temperature and fuel concentration distributions in the combustion chamber. It can be seen that the overall behaviours of these quantities are captured quantitatively in the simulation, suggesting the accuracy of these CFD calculations has reached a sufficient level for practical design purposes. Here it is of particular practical importance that the change in the flame shape from a V-form in flame A to a flat shape in flame B is correctly reproduced by the LES because the location and distribution of the flame dictates many design factors such as combustor cooling and pollutant emission control, etc. The underlying physical mechanism for this flame shape change involves a fine interplay between the fluid dynamics of the fuel/air inflows and the combustor acoustics under the operating conditions of flame B [55]. This mechanism introduces a different fuel-air mixing pattern at the nozzle exit, and this is also reflected in the downstream temperature and fuel mass fraction distributions shown in **Figure 2(b)** and **(c)**. Such mutually-interacting flow and flame dynamics cannot be captured by the conventional RANS modelling paradigm, which highlights the important role that LES can potentially play in jet engine combustor design and development.

To obtain the experimental time-averaged statistics shown in **Figure 2**, a 5-Hz laser system was used [50, 51] and no time-resolved measurement was available at the time. High-speed laser facilities have advanced rapidly in recent years allowing for measurements taken at a repetition rate up to several tens of kilo-Hertz. This hardware advancement has a significant impact on turbulent combustion experiments because the large-scale structures can now be readily resolved by the measurements in both physical space and time. From a modelling perspective, these measurements largely enrich the validation data and make it possible to assess the model capabilities of capturing transient behaviours. For the present combustor, for example, the dynamic motion of the coherent vortical structure, the so-called

precessing vortex core (PVC), and the thermo-acoustic oscillation (TAO) were both identified using 10-kHz PIV measurements [52, 56]. **Figure 3** shows a typical comparison of measured and computed axial velocity spectra for two representative monitoring points (marked in **Figure 1a**) in flames A and B. These two points are located in the swirling jet and inner shear layer (between the jet and inner recirculation zone) respectively. The velocity spectra show strong dependence on the location and also behave quite differently in the two flames. The pronounced peaks correspond to the dominant frequencies for the PVC and TAO. These frequencies with their respective amplitudes are captured reasonably well in the simulation despite a considerable under-estimation of the PVC frequency for flame A. This suggests that the LES modelling framework and the FlaRe combustion submodel described in Section 2 are adequate to capture the complex flow/flame/acoustic dynamics in this dual-swirl combustor, which are similar to those occurring in real gas turbine combustors.

As modern jet engines operate at fuel lean conditions to achieve low emissions, the flame is prone to local extinctions or even complete blow-off in the worst scenario. Such events are disastrous when occurring at high altitudes, where the engine is difficult to relight due to the low temperature, pressure and O_2 level environment. Therefore, the physical mechanism driving flame blow-off deserves a better understanding, which helps to develop not only control strategies but also predictive CFD tools for the engine design. To this end, the approaching blow-off flame C in **Table 1** was investigated experimentally by Stöhr et al. [54]. It was observed that the flame was highly unstable exhibiting sudden lift-off events with vanished flame root. Recently, this flame has been tackled using LES with FlaRe [57] and CMC [58] subgrid combustion closures, both showing a good agreement between the simulation and experiment for the flow and flame statistics. Although the flame root dynamics associated with the PVC motion was captured by both combustion models, the extreme lift-off event was only shown in the study using FlaRe [57]. This is probably due to the limitation of non-premixed CMC with a single conditioning variable-mixture fraction, while the flame root experiences strong partially premixing effects during lift-off [59]. To illustrate this lift-off event in a clear manner, **Figure 4** depicts the typical computed (using FlaRe [57]) and measured [54] flame roots for a stable instant at $t = 0$ ms and an extinguished instant at $t = 40$ ms. Despite the qualitative nature of this comparison, the simulated flame root behaviour agrees quite well with that measured using high-speed OH-PLIF and details can be found in [57]. Remarkably, the flame root extinction is successfully captured by an unstrained flamelet model, which suggests that the subgrid straining effect is not of leading order in the extinction process. This has a further implication that the cost-effective flamelet models can be used for

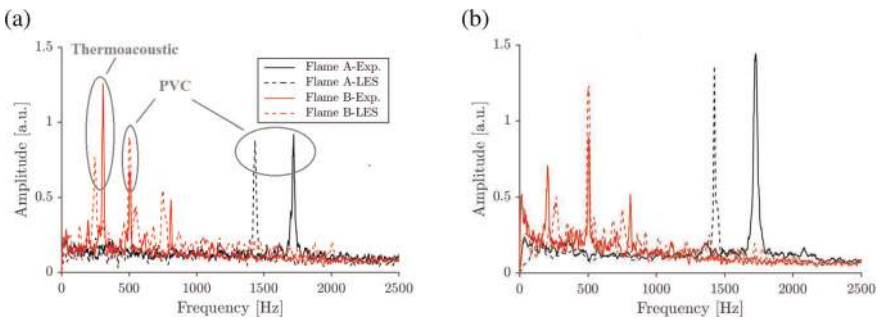

Figure 3.
*Comparison of axial velocity spectra for two monitor points (marked in **Figure 1a**) located in: (a) swirling jet and (b) inner shear layer near the nozzle exit.*

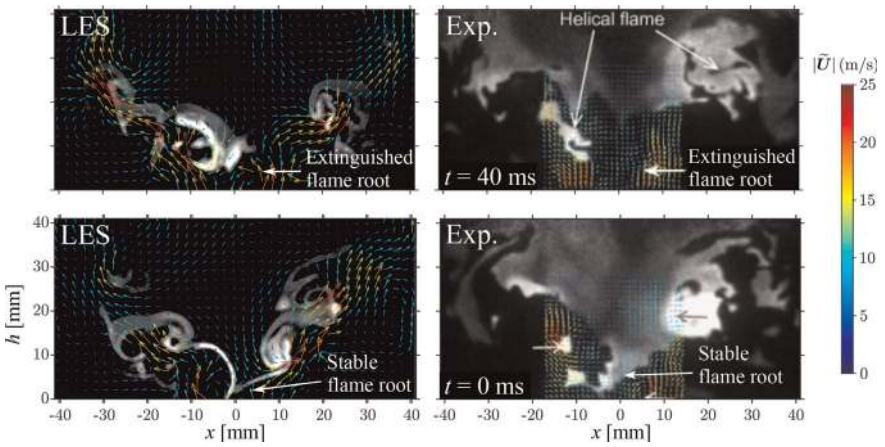

Figure 4.
LES [57] and experimental [54] snapshots of flame root overlaid by velocity arrows (coloured by magnitude) for typical stable (lower row) and extinguished (upper row) instants. The computed and measured flame is illustrated by filtered reaction rate contours and OH-PLIF images respectively.

prediction of blow-off, which itself is a slow (usually hundreds of ms) and hence computationally expensive process to simulate for practical combustor conditions.

3.2 Multi-burner annular combustor

In most modern jet engines, multiple burners are aligned circumferentially to achieve high thermal power within a compact volume. As a result, the unsteady heat release of these individual flames interact with the annular geometry of the combustion chamber, which gives rise to self-excited azimuthal instabilities [60]. Compared to longitudinal modes observed for a single flame, e.g., flame B of the DLR dual-swirl burner discussed earlier in this section, azimuthal modes are more dominant and destructive in practical applications because the circumference is usually shorter than the longitudinal length of the combustor resulting in higher resonant frequencies [61]. Thus, azimuthal instability is recognised as a primary issue for jet engine manufacturers.

Due to the complexity and high cost, only few laboratory model annular combustors have been studied experimentally so far, e.g., [62, 63], and the numerical works are scarce. To bridge this gap and gain physical insight into azimuthal instabilities, the annular burner of Worth et al. [62, 64] is simulated using the FlaRe model in this subsection. A photograph along with the schematic of this burner is shown in **Figure 5**. Fully premixed ethylene-air mixture was supplied at the bottom of the plenum and then passed through a honeycomb flow straightener before splitting into 12 bluff-body tubes by a hemispherical flow divider. Both swirling [62] and non-swirling [64] cases were investigated with and without the swirlers below the bluff-bodies. The experiments were operated at room temperature and atmospheric pressure. A bulk mean velocity evaluated at the bluff-body exit was kept constant at 18 m/s for all cases and pronounced azimuthal instability was observed for equivalence ratio ranging from $\phi = 0.8$ to 1.0. Three pressure transducers, denoted as P1, P2 and P3, were mounted on the tube wall 45 mm upstream of the bluff-body exit and they were separated by 120° to measure the azimuthal pressure waves travelling in the θ-direction.

The typical computed flame structures of the non-swirling and swirling cases for $\phi = 0.8$ are presented in **Figure 6** using volumetric rendering of the reaction rate for the 12 burners. The instantaneous axial velocity field is also shown for the mid-

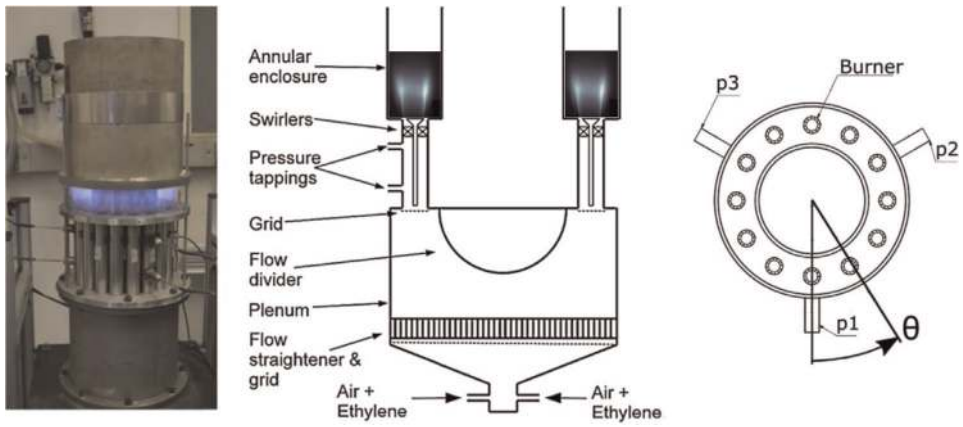

Figure 5.
Photograph and schematic of the annular combustor [62, 64].

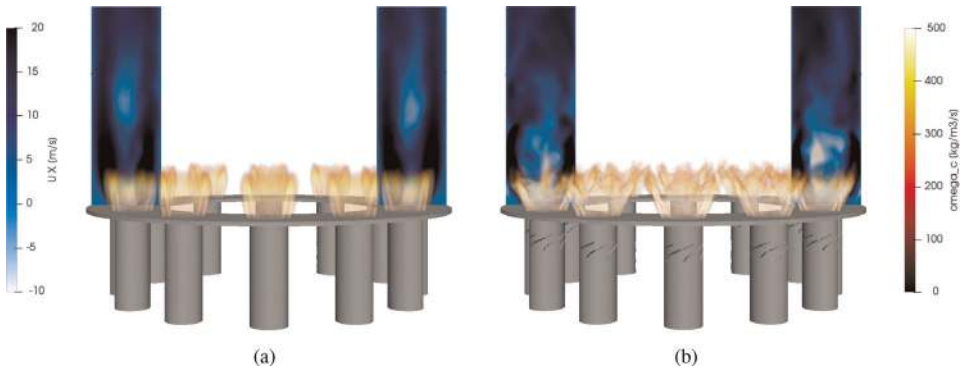

Figure 6.
Instantaneous reacting flow heat release volume rendering along with representative axial velocity contours for the (a) non-swirling and (b) swirling cases. Bulk mean velocity is $U_b = 18$ m/s with the equivalence ratio of $\phi = 0.8$.

plane of two opposed burners on the circumference. As expected, the swirl flames in **Figure 6(b)** are more compact having smaller flame lengths compared to the bluff-body flames in **Figure 6(a)**. Also, these flames are more opened up in the radial direction leading to shorter flame-to-flame distances. To qualitatively assess the LES results, **Figure 7** compares the measured and computed overhead line-of-sight integration of the mean heat release rate. In general, the distribution of the

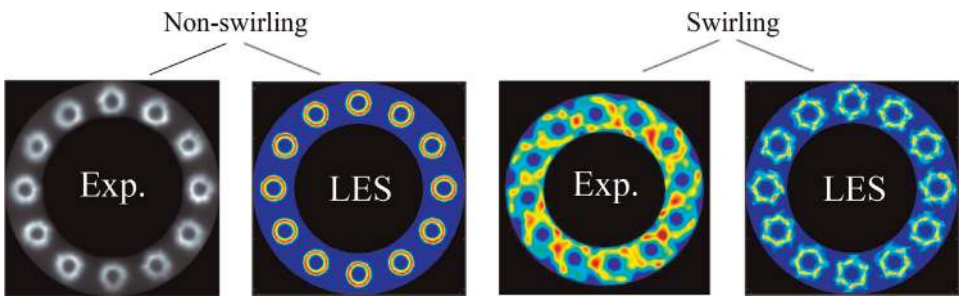

Figure 7.
*Overheard view of the line-of-sight (integrated in the axial direction) mean heat release rate for the non-swirling and swirling cases. Operating conditions are the same as in **Figure 6**.*

measured OH* signal, due to its more diffusive nature as light emissions, are more spread than the computed heat release rates for both cases with and without the swirlers. Otherwise the simulation results agree quite well with the measurements. The non-swirling flames are more or less symmetric across the annular chamber while the swirling ones clearly show a bulk swirl moving in the anti-clockwise (ACW) direction. This trend is qualitatively captured in the LES as seen in the figure.

Given that the good performance shown earlier for the single burner, it is not surprising that structure of the multiple flames is also well captured. The more important aspect of using LES for full-annular combustor is to examine its ability to predict the azimuthal instability, which is not present in single burners. This is of particular interest for the gas turbine industry because such a predictive tool which provides good accuracy at reasonable computational cost is highly needed but yet to be developed. **Figure 8** presents the typical pressure fluctuation time series taken at the three probes (marked in **Figure 5**) and their spectra for the non-swirling case with $\phi = 0.9$ and $U_b = 18$ m/s. A very clear azimuthal wave motion is seen as the p' signals of P1, P2 and P3 are exactly 120° out of phase. The computed frequency of this mode is about 1950 Hz, which agrees very well the measured value of about 1920 Hz. The small difference in the frequency could result from the adiabatic wall conditions assumed in the LES, leading to a higher speed of sound than that in the experiment with wall heat losses.

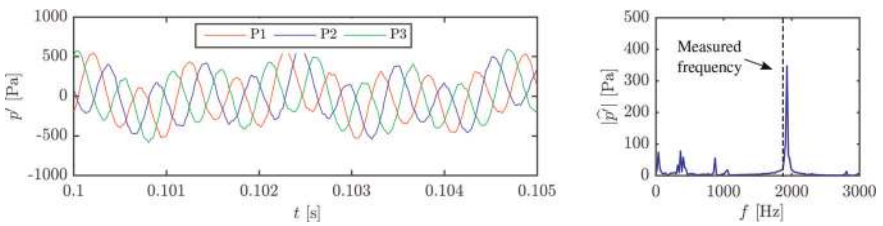

Figure 8.
*Pressure fluctuation time series (left) and power spectra (right) for the non-swirling case with $\phi = 0.9$ and $U_b = 18$ m/s. the pressure probe locations are marked in **Figure 5**.*

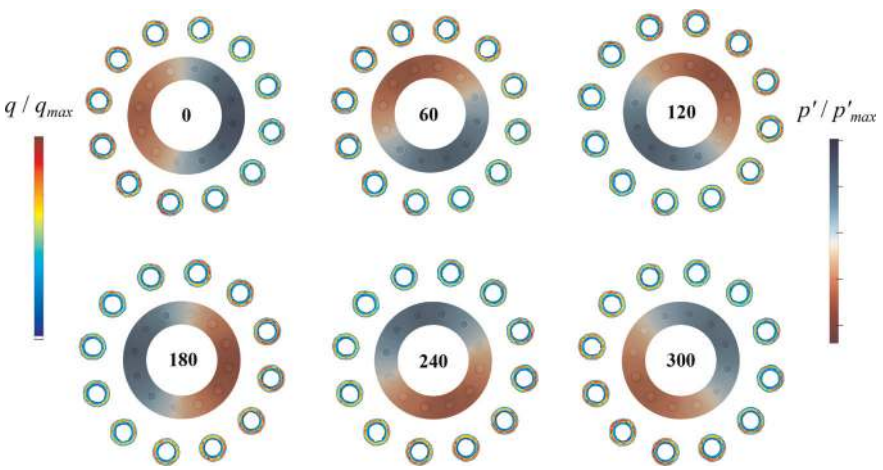

Figure 9.
Six phase angles of the azimuthal ACW spinning mode and phase-averaged heat release rates (integrated in the streamwise direction) in the transverse plane.

The pressure-heat release coupling is an essential mechanism for thermo-acoustic instabilities to occur. Thus, phase-averaged results are informative and often used to study modal behaviours of the instabilities. **Figure 9** shows the transverse-plane pressure oscillation and phase-averaged heat release rate at six different phase angles spanning over a thermo-acoustic cycle. The heat release contours are integrated values in the streamwise direction. It can be clearly seen that there is a substantial azimuthal variation in both the pressure and heat release fields. These fluctuations are strongly in phase and their peak magnitudes spin along the combustion chamber annulus at the speed of sound as also seen in the experiments [64]. However, unlike in the experiments, there is no mode switching behaviour (change of spinning direction or to standing mode) observed within the duration of the LES for this case. Such modal dynamics were detected at very low frequencies (less than 5 Hz) which require excessively long simulation runtime. This aspect is still beyond the capacities of the current petascale high-performance computing and will probably become possible in the near future as we approach the exascale era. Nonetheless, these results demonstrate that the FlaRe modelling framework used can accurately capture the major characteristics of azimuthal mode instability in annular combustors without any tuning of the model parameters. This successful LES exercise is among the firsts of its kind for the self-excited azimuthal instability in a full-annular combustor, and it is only possible when a robust, accurate and computationally inexpensive combustion model is appropriately coupled with the CFD solver. This modelling framework validated using laboratory cases in this section is readily applicable for practical combustors, which are discussed next.

4. Practical combustors

Practical combusting devices operate at high pressures, which can range from few bar for a compact power plant combustor to 30 or 40 bar for an aero engine at take-off conditions, with shaft power of the order of 100 kW to Megawatts per combustion sector. Higher powers are achieved using multi-sector and/or annular configurations. The need for high pressures lies in the efficiency of the Brayton cycle, which is the thermodynamic cycle that represents the functioning of a gas turbine. The operating principle is simple and is represented on the temperature-entropy plane in **Figure 10(a)**. The same cycle is sketched using the gas turbine components in **Figure 10(b)**. Combustion happens between points 2 and 3 of the

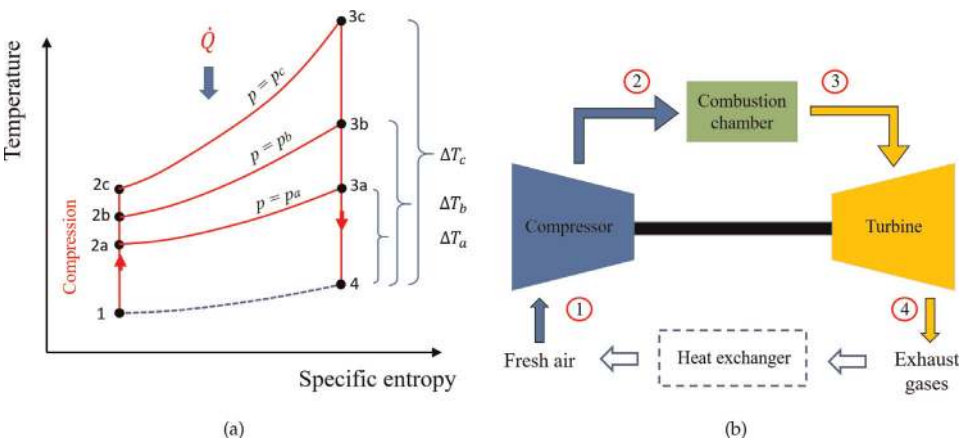

Figure 10.
Typical Brayton thermodynamic cycle for gas turbine: (a) temperature-entropy diagram and (b) sketch of the cycle components.

cycle, where chemical energy is converted into thermal energy. The gas pressure remains almost constant during this process and thus the corresponding curves on the $T - s$ plane are isobaric, and they diverge from each other as the initial temperature increases (points 2a to 2c in **Figure 10a**). This increase of temperature at point 2 of the cycle is achieved by corresponding increase in pressure by the compressor. The energy gain in terms of thermal energy can be quantified for a perfect gas by the variation of sensible enthalpy $dh_s = C_p dT$. Because of the divergence of the isobaric curves, an increase of temperature (or equivalently pressure) at the combustor entrance results in larger and larger gain of temperature and thus thermal energy at the combustor exit, point 3. For example, increasing the temperature of a quantity ΔT_i from point 2a to point 2b, results in a temperature gain $\Delta T_b - \Delta T_a > \Delta T_i$ at the combustor exit, i.e., the energy gain is larger than the amount that the turbine has to absorb to allow the compressor to yield the initial temperature increase. In other words, the higher the initial temperature (thus the pressure at point 2), the higher the energy gain, given by the thermal energy in output less the part needed by the turbine to run the compressor. There are however technological limitations for which the pressure at point 2 cannot be increased over a certain threshold, neither the temperature at point 3 can surpass a value given by structural limitations of the turbine blades, and these limitations are not going to be discussed here. It is worth mentioning that in the above discussion: (i) the cycle is ideal, i.e., irreversible losses were not taken into account; and (ii) the energy conversion between points 4 and 1 is conceptually represented by a heat exchanger and an equivalent isobaric curve. This can actually be present in a power plant where gases are recycled, but is only nominal in an aero engine, where the exhaust gases leave the system.

The design of high-pressure devices is complicated by the difficulty of having accurate measurements, in particular for temperature, on which the design process strongly relies. Non-intrusive laser techniques like Raman or Rayleigh scattering are very expensive at high pressures, and additional challenges exist because of safety reasons associated to creating an optical access in the pressurised combustion chamber area [65]. Moreover, sophisticated laser diagnostic techniques such as coherent anti-Stokes Raman spectroscopy (CARS), Raman or Rayleigh scattering may become less reliable for high pressure conditions. Several challenges exist also in numerical simulations. First, validation data from experiments is very limited for the reasons above, and this slows down the process of developing robust CFD tools to be used for the design process. Secondly, the flame thickness decreases by one or two order of magnitude as the pressure increases, about 1/10 or 1/100 of a millimetre. Given the complex geometry of modern combustion systems and their dimension which is of the order of tens of centimetres, it follows that to fully capture the small-scale combustion processes in a 3D CFD simulation the numerical grid becomes of order of hundred of millions cells. This is challenging for industrial purposes, where results are expected in order of days, despite the recent advances in high-performance computing technology, and even unaffordable when unsteady phenomena such as combustion instabilities are present, and relatively fast methods like RANS cannot be used or are unreliable. Unfortunately these instabilities are of paramount importance and their behaviour has to be understood before lean-operating, new generation engines can be developed. In this scenario it is clear that:

1. CFD modelling and in particular subgrid modelling for LES assumes a critical role to compensate for the experimental limitations and at the same time provide answers to the behaviour of unsteady phenomena such as combustion instability and local extinctions occurring in developmental combustion systems. The role of the turbulence-combustion interaction modelling is even

more critical to reduce to a minimum the mesh size and thus the simulation cost and runtime. In fact, reducing the mesh size to values of industrial practicality (order of 10 million or less) unavoidably implies that the local cell size is of order or larger than the flame thickness. It follows that the small scale processes have to be entirely modelled, which emphasises the role of the SGS modelling on the final results;

2. For a fixed mesh size, the CFD modelling has to be computationally fast. This drives the industrial choice towards specific types of modelling. In particular, flamelet-like models have attracted the interest of industries such as Rolls-Royce and Siemens for their advantages in terms of computational time (see Section 2). The limitations associated to flamelet assumption, however, lead to the need of further model development before this type of modelling can be effectively employed for design purposes.

The following subsections illustrate advantages and limitations of flamelet modelling for high pressure configurations in lean combustion systems, in light of recent CFD advancements. This is first shown for a power plant gas turbine operating at moderate pressure, where a good set of measurements and data from different combustion modelling is available for comparison. Then higher pressure configurations of aeronautical relevance are shown. These cases are chosen as they provide some limited but valuable experimental data for validation purposes.

4.1 Siemens combustor for energy generation

The following combustor sector is a modified version of the commercial SGT-100 family of Siemens, which consists of 6 combustors delivering a nominal shaft power of 5.7 MW. Each combustor burns natural gas after mixing with air in the swirler and prechamber of the geometry, shown in **Figure 11(a)**. The burner operates at 3 bar pressure, which is above atmospheric conditions, but is relatively low to allow a large database of in-flame measurements to be available for model validation, including temperature, velocity and major and minor species mass fractions radial profiles at four axial locations [67]. This configuration is swirled and features a PVC, which can be identified by looking at the velocity contours in the combustor primary zone in **Figure 11**. The stagnation point, marked in the figure, is in fact not on the centreline, suggesting that the PVC did not complete an entire

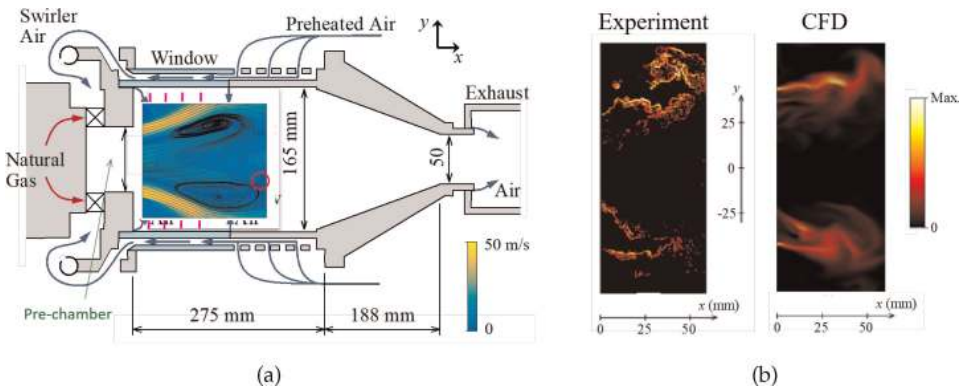

Figure 11.
Non-to-scale representation of the Siemens SGT-100 combustor with dimensions and velocity magnitude contours and streamlines from PIV measurements [22, 66] in the primary (combusting) zone) (a). The experimental and numerical flame are shown in (b) for a random instant of time.

revolution, and this has an effect on the statistics. The existence of a PVC is common in lean combustion burners and thus has to be taken carefully into account before comparisons are made with CFD results. Also, the PVC is usually coupled with the system acoustics, although this will not be discussed in the merit for this case. In addition to the PVC, the central recirculation zone, represented by the two large vortices in the figure, is strongly dependent on the jet angle at the exit of the prechamber, which thus affects the axial position of the stagnation point and, in turn, the statistics. These characteristics make the Siemens SGT-100 combustor a challenging case for model validation, which is useful to understand model advantages and limitations. These are discussed in light of recent modelling advances next.

The Siemens configuration has been investigated numerically using different LES combustion modelling, including TPDF/ESF [68], partially stirred reactor (PaSR) [69], TF [70, 71], FlaRe [22], eddy dissipation, fractal and approximate decomposition models [71]. Comparisons among different modelling techniques are also shown in [22, 71]. The combustion conditions for the Siemens configuration were noted in [67] to lie between thin and distributed reaction zones regimes of the turbulent combustion diagram [72]. According to this, the smallest turbulent eddies are able to penetrate the internal flame structure, thus invalidating the flamelet hypothesis. However, detailed interrogation [69] of the measured OH suggested that there were flamelets embedded in an environment of distributed combustion, i.e., flamelet structures and thus flamelet modelling are still possible at high Karlovitz number regimes, which was observed also for other configurations [36]. The Siemens configuration is thus a critical case as it opens the way to exploit the strong computational advantage of flamelets for highly turbulent, high pressure configurations typical of practical burners. As discussed earlier, there are two ways of proceeding to simulate a high pressure flame. One way is to decrease the cell dimensions (thus increase the mesh count) so that at least 5–10 numerical cells lie within the flame thickness and consequently a good part of the turbulence-flame interaction is captured at the resolved level in the LES. This decreases the impact of the SGS modelling on the statistics. Nevertheless, as explained earlier this is unpractical. The second approach is to have a coarser, affordable mesh size, with the SGS modelling playing a strong role. As combustion is a small scale process, this strongly reflects on the statistics, which is illustrated in **Figure 11(b)**. As the mesh is not fine enough to enter the flame structure, the numerical flame appears smoothed and filtered in respect to the experimental one, where the wrinkling effect of small vortices is observable. The big challenge is thus to have a modelling which, despite the inability to represent this at the resolved level, is able to capture the effects on a number of statistics (first and second moments, PDFs, etc.) and remain computationally cheap at the same time. The simulation cost for the Siemens combustor starts from about 550 CPU-hour per ms of simulation for a flamelet model and can increase significantly depending on modelling and grid size, although precise values were not reported for other combustion models used for the same configuration [68–71].

The performance of the FlaRe model discussed in Section 2 and its ability to predict the flow field characteristics can be assessed by comparing the CFD results to experimental data available for the Siemens configuration [67]. Typical comparisons of radial profiles of temperature and velocity are shown in **Figure 12** for two axial locations in the flame region (please refer to [22] for a full database of comparisons). The first location is about 19 mm downstream the pre-chamber exit, where the flow diverges due to the sudden expansion and the second is 70 mm further downstream, where the gases are close to burnt conditions. Velocity and its rms are predicted with good accuracy by the LES at the upstream position, but some mis-alignment of the peak values is observed for the mean velocity at the

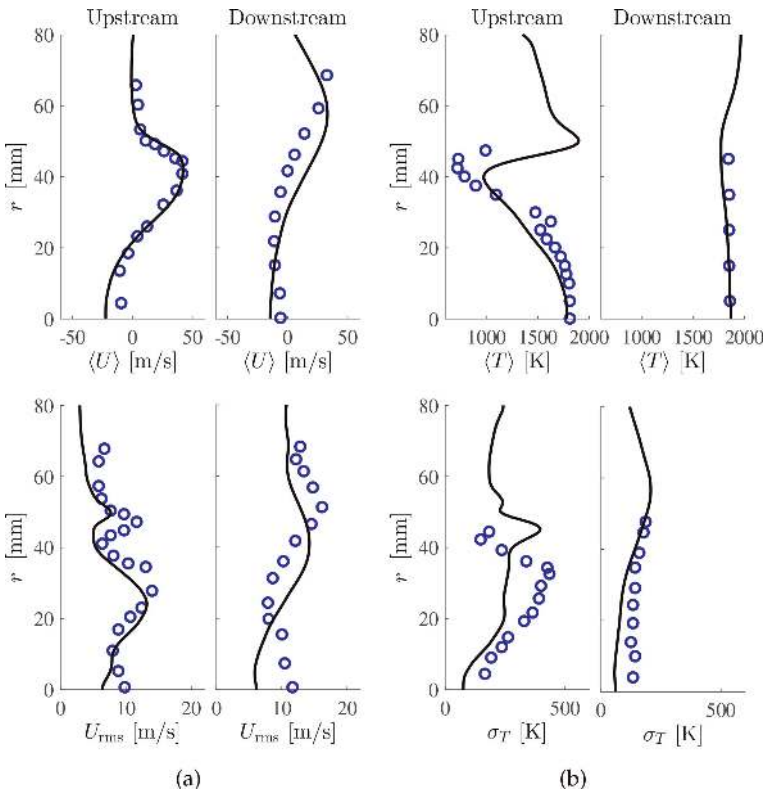

Figure 12.
Radial profiles of mean axial velocity, U (a), temperature, T (b), and their rms values at two axial positions in the primary zone of the SGT-100 combustor. Measurements (circles) are compared with LES results using FlaRe approach.

downstream position, which in turn affects the rms field. This is partly due to the fact that the LES is slightly over-predicting the jet angle at the combustor entrance (see **Figure 11**), which is also observed in predictions from other combustion models. Temperature profiles at the most upstream position show that the LES-FlaRe approach captures this quantity satisfactorily except for some over-prediction at $r \approx 40$ mm. This is the region where the flame anchors and is subjected to strong effect of strain [70]. It is possible that the grid resolution at this location needs further refinement to capture this effect at the resolved level. Similar over-predictions were observed using the TF approach with a similar grid resolution in [71]. While an improved accuracy was shown for TF model in [70] using 120 M cells increasing non-negligible computational cost, this may not be affordable for routine in-house calculations in industries. The work in [69] using PaSR model also shows that chemistry and in particular extinction strain rates may also play an effect at the same radial location (see also discussion in [22]). At the downstream locations where gases are burnt the temperature is predicted very well by the LES-FlaRe model, which is also a consequence of the fact that flamelet models guarantee that the correct adiabatic value is approached in burnt conditions, which may not be true for other modelling approaches. This is particularly relevant for real engines configurations where correct predictions of temperature and composition at the exhaust are needed for design purposes. The temperature rms also is satisfactorily predicted. It is worth mentioning that the heat released at the SGS scales has a strong effect on temperature and thus the portion of SGS temperature variance is large as compared to the resolved variance. Further modelling development is necessary to predict temperature fluctuations at SGS level. Prediction of

temperature variance may become particularly relevant in situations where the measurement data is not density weighted (not the case for the Siemens combustor shown here, where measurement data is density weighted). As the reacting Navier-Stokes equations are density weighted, in such a case the LES data should be processed to obtain non-weighted averages using an approximation. This approximation will involve the estimation of the total variance (resolved plus SGS), as shown for example in [20]. The development of modelling to account for the SGS temperature variance in the statistics deserves thus a larger attention than that demonstrated in recent years.

Overall the flamelet model predictions are satisfactory and of similar accuracy than those obtained by other modelling approaches, at a significantly lower computational cost. Increase in accuracy can be achieved either increasing the mesh size (resolving more and more of the small-scale turbulence-flame interaction processes) or acting on the chemical mechanism (see discussion in [22] for more details), with different modelling giving similar performance at equal conditions of mesh and chemistry resolution. The recent advances in modelling development and in particular the progresses in the turbulence-reaction-dissipation balance have allowed flamelets to cover the gap that separated them from other modelling approaches. Also, the fully detailed mechanism used by flamelet models potentially allows to have information on more chemical species than in other models at no additional cost, as long as the correct flame-turbulence interaction is predicted. Note that this still does not imply that flamelet will be successful at higher pressures as the Siemens case clearly indicates that limitations exist in all combustion modelling when the LES filter size is larger than the flame thickness. The following subsection will shed some light on this.

4.2 Aero engine configurations

The lack and cost of experimental data, and the limitations of most combustion models to simulate complex high-pressure configurations in times affordable by industry, have slowed down the process of development of lean combustor technology. Flamelets models are computationally cheap enough to be used in industry but up to recently they have not been considered sufficiently accurate to be employed for high turbulence, high Karlovitz conditions for gas turbine combustion. The recent advances in flamelet modelling in the context of LES and the better understanding of the small-scale interaction between turbulence, reaction and diffusion as discussed in the previous sections, have shown potential to overcome the limitations of flamelets modelling and thus open the way to a faster design process.

In aero engines there is an additional modelling issue to consider which is due to the liquid fuel, usually kerosene or similar, which brings the modelling of the two-phase flow, fuel droplets break-up and their evaporation into consideration. These brings additional parameters and degrees of freedom in the CFD modelling and thus measurements of spray statistics such as Sauter mean diameter (SMD) and droplet velocity are needed to reduce the uncertainty in comparing CFD and experimental data. The spray behaviour, in general, both affects and is affected by the velocity and temperature field and thus it is not simple to separate spray and reaction effects. The validation of CFD models in aero engines thus leads to different considerations depending on whether the investigated region is close to the injectors or not.

4.2.1 Comparisons in the primary zone

The following test case is representative of a single sector aero engine combustor, where the spray statistics were observed to be only slightly affected by the

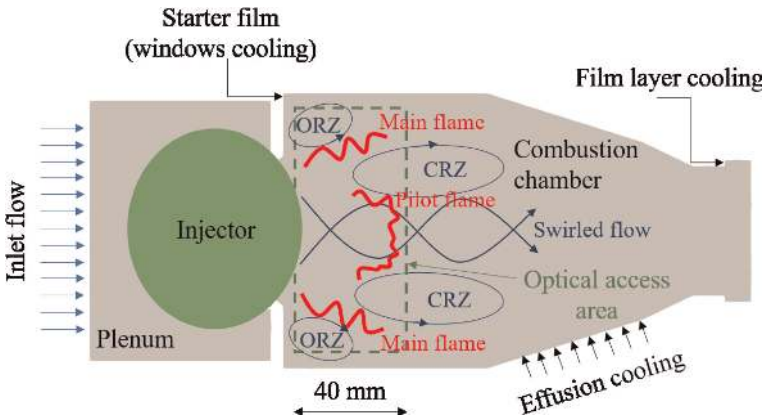

Figure 13.
Sketch of the pressurised BOSS rig of DLR operated with a Rolls Royce fuel injector.

surrounding field. A sketch of this combustor is shown in **Figure 13**. Pressurised air in the order of 10 bar and preheated at temperature T_{30} of about 700 K flows through a burner which consists of two stages: a central, pilot stage and a surrounding main stage. There are swirlers in each of these passages. These flow paths are designed to deliver different flow splits, and can have different channels of co-rotating or counter-rotating flows depending on the particular injector geometry and configuration. Liquid fuel is injected before the combustor entrance from the injector edges and is also split into pilot and main stages. The fuel split depends on the desired power settings (take-off, approach, idle, etc.). Correspondingly, the flame also consists of pilot and main branches, respectively stabilised in the internal part of the central recirculation zone (CRZ), and between the CRZ and the outer recirculation zone (ORZ) forming as consequence of the sudden expansion of the swirling flow at the chamber entrance. Film and effusion cooling are used to protect the walls from the high temperature gases in both primary and secondary zones. Previous studies [23] have shown that the spray statistics are not strongly influenced by the surrounding flow field in this configuration, so this case offers a good opportunity to evaluate the combustion model performance independently of the spray modelling. The computed SMD and droplet velocities were shown to compare well with measurements in [23]. When it comes to compare fields like temperature, the difficulties in having reliable measurements in the flame region lead, in the few cases where measurements are available at high pressure conditions, to significant uncertainties and this slows down the validation process of CFD models. For the studied configuration, direct measurements of OH concentration are available, with an uncertainty of 20–30% [73]. As other intermediate species, OH can be used to have a qualitative picture of the flame configuration and thus this quantity is still valuable for CFD validation purposes. Typical comparisons of OH mass fraction with LES-FlaRe predictions are shown for the primary zone in **Figure 14a**. Qualitatively, the LES-flamelet approach shows to be able to predict the correct flame configuration, involving a penetrating pilot (central) jet. This is challenging as an incorrect balance of reaction and turbulence can result in a completely different configuration with a diverging pilot jet and a flame anchored upstream in a V-shape [23]. Quantitatively, the OH concentration from the LES can over-predict that from experiment of a factor of two or larger as observed in the figure. However, this has to be carefully interpreted due to the uncertainty in the measurement and considering that the real objective is to predict temperature. This has a favourable non-linear dependence on OH (OH increases exponentially with

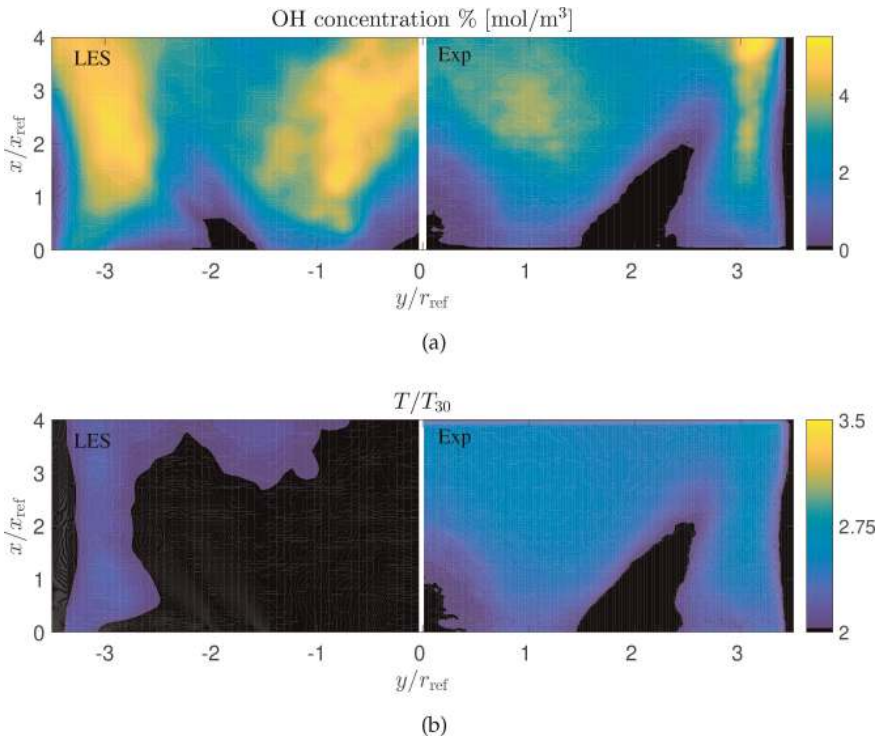

Figure 14.
Comparison of mean OH concentration (a) and temperature (b) from LES and measurements (for temperature) in the mid-plane of the primary zone of the Rolls-Royce Boss-rig. The temperature is normalised by the inlet temperature, T_{30}, for confidential reasons.

temperature) and thus the differences observed in **Figure 14a** are expected to become much smaller in terms of temperature. Unfortunately, direct measurements of temperature at high pressure condition are challenging as explained earlier and this quantity is if often estimated indirectly by making additional assumptions, which in turns lead to additional uncertainty. For example, for the combustor test case investigated here temperature can be estimated from OH concentration via equilibrium assumption [73]. A direct comparison of the experimental temperature in this case with that obtained in the LES from Eq. (7) can lead to incorrect conclusions if the underlying assumptions used in the experimental data are not carefully taken into account. An example of this is shown in **Figure 14b**, where the LES temperature appears to be significantly under-estimated in respect to that from experiments in the pilot flame region. This would be inconsistent to the behaviour observed for **Figure 14a** and suggests that comparisons of temperature in the burner primary region have to be assessed with due care at high pressure conditions.

4.2.2 Comparisons at the combustor exit

Comparisons between LES and measurements are more meaningful at the combustor exit where the gases are almost entirely combusted and thus assumptions such as that of chemical equilibrium are expected to better hold. Also, measurements at the combustor exit are as important as those in the primary region as the flow field here is the result of what happens upstream. Thus, experimental data at the combustor exit can be used for model validation with an increased degree of

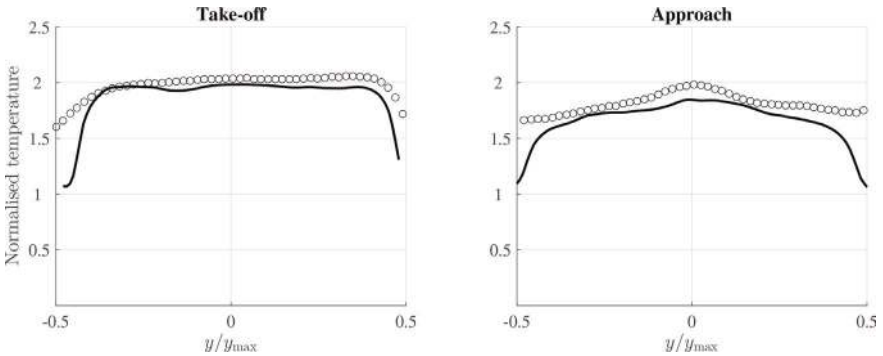

Figure 15.
Comparison of temperature profiles from measurements (symbols, courtesy of DLR Cologne, Germany) and LES (lines) at the exit plane of the DLR OCORE-2 rig of a practical single-sector aero engine combustor for two operating conditions.

quantitativeness in comparison to the primary zone. Measurements at the burner exit are not available for the configuration investigated in the previous section; however, temperature measurements are available for a similar rig, featuring a similar injector and the same flow configuration of **Figure 13**. Comparisons between experimental data and FlaRe-LES results are shown in **Figure 15** for two operating conditions at the same pressure and inlet temperature, but different flow split. These configurations are representative of approach and cutback conditions of an airplane. The differences observed near the walls of the combustor ($y/y_{\max} = \pm 0.5$) are due to the effusion cooling that lowers the temperature below the minimum detectable from the experiment (about 1200 K). Except for this region, the FlaRe model prediction matches very well that from experiment, which shows that this type of modelling is capable to represent the correct statistical behaviour even at high pressure when the intricate balance between turbulence, dissipation and heat release is correctly taken into account. Recent advances in the modelling in context of flamelets are thus promising for future design cycles of aero engines, although additional validations are still needed.

5. Summary and future outlook

In this chapter, an overview for the current status of the use of combustion CFD in modern gas turbine engine combustor design is presented. There is a general tendency in the industry to move from the conventional RANS to the more powerful LES modelling paradigm, and thus the discussion is focused on the application of LES. The various challenges for LES modelling of gas turbine combustion are discussed and a number of representative subgrid combustion models are briefly described. Flamelet approaches are more attractive for industry because of their significantly higher computational efficiency and relatively simple implementation in different CFD codes. The particular focus was given to a recently developed model called FlaRe, which is a revised flamelet approach keeping the physical consistencies among various SGS models and physical processes. To assess the performance of FlaRe, the LES results are compared with experimental measurements for several typical laboratory and practical combustors. A broad range of phenomena of high practical interest are involved in these test cases including flame-vortex interaction, self-excited thermoacoustic oscillations, flame root dynamics close to lean blow-off, high pressure conditions, liquid fuel combustion, etc.

The combustion regimes involved span over the full range for practical jet engine conditions involving premixed, non-premixed and a mixture of both. An overall good agreement between simulation and experiment is observed across all cases presented. This suggests that despite the limitations of the fundamental flamelet concept, which many believe is far from being valid for real industrial conditions, there is a great potential for flamelet models to be used in the industry on a frequent basis because of its computational efficiency, robustness and improved accuracy if the consistencies are maintained. This modelling framework is yet to be extended to cover other important aspects such as non-adiabatic effects, pollutant emission, autoignition, etc., of a real engine combustor.

Acknowledgements

The authors IL and NS thank the DLR Institute of Propulsion Technology in Cologne for kindly providing measurement data for some of the figures shown in this chapter, and in particular Dr C. Willert, Dr T. Behrendt and Dr J. Heinze for their useful advice on Section 4.2. The support from Mitsubishi Heavy Industries, Takasago, Japan is acknowledged by ZXC and NS. The presented simulations used the ARCHER UK National Supercomputing Service and the CSD3 Cluster of Cambridge University.

Author details

Zhi X. Chen[1*], Ivan Langella[2] and Nedunchezhian Swaminathan[1]

1 Department of Engineering, University of Cambridge, Cambridge, UK

2 Department of Aeronautical and Automotive Engineering, Loughborough University, Loughborough, UK

*Address all correspondence to: zc252@cam.ac.uk

References

[1] Lefebvre AH, Ballal DR. Gas Turbine Combustion: Alternative Fuels and Emissions. Boca Raton, USA: CRC Press; 2010

[2] Poinsot T, Veynante D. Theoretical and Numerical Combustion. 2nd ed. Philadelphia, USA: Edwards; 2005

[3] Pope SB. Turbulent Flows. Cambridge, UK: Cambridge University Press; 2000

[4] Gicquel LYM, Staffelbach G, Poinsot T. Large Eddy simulations of gaseous flames in gas turbine combustion chambers. Progress in Energy and Combustion Science. 2012;**38**:782-817

[5] Pitsch H. Large-Eddy simulation of turbulent combustion. Annual Review of Fluid Mechanics. 2006;**38**: 453-482

[6] Smagorinsky J. General circulation experiments with the primitive equations. Monthly Weather Review. 1963;**91**(3):99-164

[7] Langella I, Doan NAK, Swaminathan N, Pope SB. Study of subgrid-scale velocity models for reacting and nonreacting flows. Physical Review Fluids. 2018;**3**:054602

[8] Swaminathan N, Bray KNC, editors. Turbulent Premixed Flames. Cambridge, UK: Cambridge University Press; 2011

[9] Colin O, Ducros F, Veynante D, Poinsot T. A thickened flame model for large eddy simulations of turbulent premixed combustion. Physics of Fluids. 2000;**12**:1843

[10] De A, Acharya S. Large Eddy simulation of a premixed Bunsen flame using a modified thickened-flame model at two Reynolds number. Combustion Science and Technology. 2009;**181**: 1231-1272

[11] Janicka J, Sadiki A. Large eddy simulation of turbulent combustion systems. Proceedings of the Combustion Institute. 2005;**30**:537-547

[12] Moureau V, Fiorina B, Pitsch H. A level set formulation for premixed combustion LES considering the turbulent flame structure. Combustion and Flame. 2008;**156**:801-812

[13] Pitsch H. A consistent level set formulation for large-eddy simulation of premixed turbulent combustion. Combustion and Flame. 2005;**143**: 587-598

[14] Dunn MJ, Masri AR, Bilger RW, Barlow RS, Wang GH. The compositional structure of highly turbulent piloted premixed flames issuing into a hot Coflow. Proceedings of the Combustion Institute. 2009;**32**: 1779-1786

[15] Poludnenko AY, Oran ES. The interaction of high-speed turbulence with flames: Global properties and internal flame structure. Combustion and Flame. 2010;**157**:995-1011

[16] Temme JE, Wabel TM, Skiba AW, Driscoll JF. Measurements of premixed turbulent combustion regimes of high Reynolds number flames. In: 53rd AIAA Aerospace Sciences Meeting. AIAA. Kissimmee, Florida: American Institute of Aeronautics and Astronautics. 2015

[17] Poinsot T, Veynante D, Candel S. Quenching processes and premixed turbulent combustion diagrams. Journal of Fluid Mechanics. 1991;**228**: 561-606

[18] Roberts WL, Driscoll JF, Drake MC, Goss LP. Images of the quenching of a flame by a vortex—To quantify regimes of turbulent combustion. Combustion and Flame. 1993;**94**:58-69

[19] Duwig C. Study of a filtered flame formulation for large eddy simulation of premixed turbulent flames. Flow, Turbulence and Combustion. 2007;**79**: 433-454

[20] Langella I, Swaminathan N. Unstrained and strained flamelets for LES of premixed combustion. Combustion Theory and Modelling. 2016;**20**:410-440

[21] Doan NAK, Swaminathan N, Chakraborty N. Multiscale analysis of turbulence-flame interaction in premixed flames. Proceedings of the Combustion Institute. 2016;**36**:1929-1935

[22] Langella I, Chen ZX, Swaminathan N, Sadasivuni SK. Large-Eddy simulation of reacting flows in industrial gas turbine combustor. Journal of Propulsion and Power. 2018;**34**: 1269-1284

[23] Langella I, Heinze J, Behrendt T, Swaminathan N, Zedda M, Voigt L. Turbulent flame shape switching at conditions relevant for gas turbines. Journal of Engineering for Gas Turbines and Power. 2019;GTP-19-1385

[24] Chen ZX, Langella I, Swaminathan N, Stöhr M, Meier W, Kolla H. Large Eddy simulation of a dual swirl gas turbine combustor: Flame/flow structures and stabilisation under thermoacoustically stable and unstable conditions. Combustion and Flame. 2019;**203**:279-300

[25] Bilger RW. Structure of diffusion flames. Combustion Science and Technology. 1976;**13**:155-170

[26] Demoulin FX, Borghi R. Modeling of turbulent spray combustion with application to diesel like experiment. Combustion and Flame. 2002;**129**: 281-293

[27] Giusti A, Mastorakos E, Hassa C, Heinze J, Magens E, Zedda M. Investigation of flame structure and soot formation in a single sector model combustor using experiments and numerical simulations based on the large eddy simulation/conditional moment closure approach. Journal of Engineering for Gas Turbines and Power. 2018;**140**:061506-061509

[28] Fiorina B, Gicquel O, Vervisch L, Carpentier S, Darabiha N. Approximating the chemical structure of partially premixed and diffusion counterflow flames using FPI flamelet tabulation. Combustion and Flame. 2005;**140**:147-160

[29] Bray KNC, Domingo P, Vervisch L. Role of the progress variable in models for partially premixed turbulent combustion. Combustion and Flame. 2005;**141**(4):431-437

[30] Bradley D, Gaskell PH, Lau AKC. A mixedness-reactedness flamelet model for turbulent diffusion flames. Proceedings of the Combustion Institute. 1990;**23**(1):685-692

[31] Salehi MM, Bushe WK, Shahbazian N, Groth CPT. Modified laminar flamelet presumed probability density function for LES of premixed turbulent combustion. Proceedings of the Combustion Institute. 2013;**34**:1203-1211

[32] Domingo P, Vervisch L, Payet S, Hauguel R. DNS of a premixed turbulent V flame and LES of a ducted flame using FSD-PDF subgrid scale closure with FPI-tabulated chemistry. Combustion and Flame. 2005;**143**: 566-586

[33] Landenfeld T, Sadiki A, Janicka J. A turbulence-chemistry interaction model based on a multivariate presumed Beta-PDF method for turbulent flames. Flow, Turbulence and Combustion. 2002;**68**: 111-135

[34] Lecocq G, Richard S, Colin O, Vervisch L. Hybrid presumed pdf and

flame surface density approaches for large-eddy simulation of premixed turbulent combustion: Part 1: Formalism and simulation of a quasi-steady burner. Combustion and Flame. 2011;**158**: 1201-1214

[35] Vreman AW, van Oijen JA, de Goey LPH. Subgrid scale modelling in large-eddy simulation of turbulent combustion using premixed flamelet chemistry. Flow, Turbulence and Combustion. 2009;**82**:511-535

[36] Langella I, Swaminathan N, Pitz RW. Application of unstrained flamelet SGS closure for multiregime premixed combustion. Combustion and Flame. 2016;**173**:161-178

[37] Chen ZX, Doan NAK, Ruan S, Langella I, Swaminathan N. *A priori* investigation of subgrid correlation of mixture fraction and progress variable in partially premixed flames. Combustion Theory and Modelling. 2018;**22**:862-882

[38] Fritz J, Kröner M, Sattelmayer T. Flashback in a swirl burner with cylindrical premixing zone. In: International Gas Turbine and Aeroengine Congress and Exhibition. ASME. New Orleans, LA: American Society of Science and Engineering. 2001

[39] Schmehl R, Maier G, Wittig S. CFD analysis of fuel atomization, secondary droplet breakup and spray dispersion in the premix duct of a LPP combustor. Proceedings of the ICLASS. 2000

[40] Pera C, Réveillon J, Vervisch L, Domingo P. Modeling subgrid scale mixture fraction variance in LES of evaporating spray. Combustion and Flame. 2006;**146**:635-648

[41] Dunstan TD, Minamoto Y, Chakraborty N, Swaminathan N. Scalar dissipation rate modelling for large Eddy simulation of turbulent premixed flames. Proceedings of the Combustion Institute. 2013;**34**:1193-1201

[42] Ruan S, Swaminathan N, Darbyshire OR. Modelling of turbulent lifted jet flames using flamelets: *A priori* assessment and *a posteriori* validation. Combustion Theory and Modelling. 2014;**18**(2):295-329

[43] TNF Workshop;. Available from: https://www.sandia.gov/TNF/abstract.html

[44] Pope SB. Small scales, many species and the manifold challenges of turbulent combustion. Proceedings of the Combustion Institute. 2013;**34**:1-31

[45] Ahmed SF, Mastorakos E. Spark ignition of lifted turbulent jet flames. Combustion and Flame. 2006;**146**(1–2): 215-231

[46] Chen Z, Ruan S, Swaminathan N. Large Eddy simulation of flame edge evolution in a spark-ignited methane-air jet. Proceedings of the Combustion Institute. 2017;**36**:1645-1652

[47] Zhang H, Giusti A, Mastorakos E. LES/CMC modelling of ignition and flame propagation in a non-premixed methane jet. Proceedings of the Combustion Institute. 2019;**37**:2125-2132

[48] Lacaze G, Cuenot B, Poinsot T, Oschwald M. Large eddy simulation of laser ignition and compressible reacting flow in a rocket-like configuration. Combustion and Flame. 2009;**156**: 1166-1180

[49] Jones WP, Prasad VN. LES-pdf simulation of a spark iginited turbulent methane jet. Proceedings of the Combustion Institute. 2011;**33**:1355-1363

[50] Weigand P, Meier W, Duan XR, Stricker W, Aigner M. Investigations of swirl flames in a gas turbine model combustor. I. Flow field, structures, temperature, and species distributions.

Combustion and Flame. 2006;**144**: 205-224

[51] Meier W, Duan XR, Weigand P. Investigations of swirl flames in a gas turbine model combustor. II. Turbulence–chemistry interactions. Combustion and Flame. 2006;**144**: 225-236

[52] Stöhr M, Boxx I, Carter CD, Meier W. Experimental study of vortex-flame interaction in a gas turbine model combustor. Combustion and Flame. 2012;**159**:2636-2649

[53] Steinberg AM, Boxx I, Stöhr M, Carter CD, Meier W. Flow–flame interactions causing acoustically coupled heat release fluctuations in a thermo-acoustically unstable gas turbine model combustor. Combustion and Flame. 2010;**157**:2250-2266

[54] Stöhr M, Boxx I, Carter C, Meier W. Dynamics of lean blowout of a swirl-stabilized flame in a gas turbine model combustor. Proceedings of the Combustion Institute. 2011;**33**: 2953-2960

[55] Chen ZX, Swaminathan N, Stöhr M, Meier W. Interaction between self-excited oscillations and fuel-air mixing in a dual swirl combustor. Proceedings of the Combustion Institute. 2019;**37**: 2325-2333

[56] Boxx I, Stöhr M, Carter C, Meier W. Temporally resolved planar measurements of transient phenomena in a partially pre-mixed swirl flame in a gas turbine model combustor. Combustion and Flame. 2010;**157**:1510-1525

[57] Massey JC, Chen ZX, Swaminathan N. Lean flame root dynamics in a gas turbine model combustor. Combustion Science and Technology. 2019. DOI: 10.1080/00102202.2019.1584616

[58] Zhang H, Mastorakos E. LES/CMC modelling of a gas turbine model combustor with quick fuel mixing. Flow, Turbulence and Combustion. 2018. DOI: 10.1007/s10494-018-9988-1

[59] Lawn CJ. Lifted flames on fuel jets in co-flowing air. Progress in Energy and Combustion Science. 2009;**35**(1): 1-30

[60] Lieuwen TC, Yang V. Combustion Instabilities in Gas Turbine Engines: Operational Experience, Fundamental Mechanisms, and Modeling. Reston, VA: AIAA Inc; 2006

[61] Dowling AP, Stow SR. Acoustic analysis of gas turbine combustors. Journal of Propulsion and Power. 2003; **19**:751-764

[62] Worth NA, Dawson JR. Modal dynamics of self-excited azimuthal instabilities in an annular combustion chamber. Combustion and Flame. 2013; **160**:2476-2489

[63] Bourgouin JF, Durox D, Moeck JP, Schuller T, Candel S. A new pattern of instability observed in an annular combustor: The slanted mode. Proceedings of the Combustion Institute. 2015;**35**:3237-3244

[64] Mazur M, Nygard HT, Dawson JR, Worth NA. Characteristics of self-excited spinning azimuthal modes in an annular combustor with turbulent premixed bluff-body flames. Proceedings of the Combustion Institute. 2019;**37**:5129-5136

[65] Kohse-Höinghaus K, Barlow RS, Aldén M, Wolfrum J. Combustion at the focus: Laser diagnostics and control. Proceedings of the Combustion Institute. 2005;**30**:89-123

[66] Stopper U, Aigner M, Ax H, Meier W, Sadanandan R, Stör M, et al. PIV, 2D-LIF and 1D-Raman measurements of flow field, composition and temperature in premixed gas turbine flames.

Experimental Thermal and Fluid Science. 2010;**34**:396-403

[67] Stopper U, Meier W, Sadanandan S, Stör M, Aigner M, Bulat G. Experimental study of industrial gas turbine flames including quantification of pressure influence on flow field, fuel/air premixing and flame shape. Combustion and Flame. 2013;**160**: 2103-2118

[68] Bulat G, Jones WP, Marquis AJ. NO and CO formation in an industrial gas-turbine combustion chamber using LES with the Eulerian sub-grid PDF method. Combustion and Flame. 2014;**161**: 1804-1825

[69] Bulat G, Fedina E, Fureby C, Meier W, Stopper U. Reacting flow in an industrial gas turbine combustor: LES and experimental analysis. Proceedings of the Combustion Institute. 2015;**35**: 3175-3183

[70] Jaravel T, Riber E, Cuenot B, Buat G. Large Eddy simulation of an industrial gas turbine combustor using reduced chemistry with accurate pollutant prediction. Proceedings of the Combustion Institute. 2016;**36**: 3817-3825

[71] Fedina E, Fureby C, Bulat G, Meier W. Assessment of finite rate chemistry large Eddy simulation combustion models. Flow, Turbulence and Combustion. 2017;**99**:385-409

[72] Peters N. Turbulent Combustion. Cambridge, UK: Cambridge University Press; 2000

[73] Heinze J, Meier U, Behrendt T, Willert C, Geigle KP, Lammel O, et al. PLIF thermometry based on measurements of absolute concentrations of the OH radical. Zeitschrift für Physikalische Chemie. 2011;**225**:1315-1341